Plasma Phys. Control. Fusion **41** (1999) A61–A73. Printed in the UK PII: S0741-3335(99)97298-6

Magnetic-field-aligned electric fields associated with Debye-scale plasma structures

R E Ergun†

Space Sciences Laboratory, University of California, Berkeley, CA, USA

Received 3 July 1998

Abstract. Quasi-static, magnetic-field-aligned (parallel) potentials have been considered the primary source of charged particle acceleration in the aurora where precipitating electrons create a visible display. This finding has been controversial since, at one time, it was widely believed that parallel potentials could not be supported by a collisionless plasma. We present observations from the fast auroral snapshot (FAST) satellite which strongly support this acceleration mechanism and, moreover, show evidence of a second plasma regime region which supports quasi-static parallel potentials. The uncovering of parallel potentials in two plasma regimes suggests that they may be fundamental in astrophysical plasmas, supplementing the classical mechanisms of Fermi and betatron acceleration. We summarize the observations that demonstrate this acceleration mechanism. We also summarize evidence of Debye-scale plasma structures which are associated with these parallel potentials. These small-scale structures appear to be three-dimensional electron phase space holes, a new type of plasma structure.

1. Introduction

In this paper, three of the important findings of the fast auroral snapshot (FAST) mission are summarized. These findings include compelling evidence that quasi-static, magnetic-field-aligned potentials are the primary acceleration mechanism of charged particles in the auroral zone [1, 2], the uncovering of a second distinct plasma regime that supports magnetic-field-aligned potentials [1, 3] and the identification of a new type of plasma structure, a three-dimensional (3D) electron phase space hole, that is associated with magnetic-field-aligned potentials [4, 5].

Quasi-static, magnetic-field-aligned (parallel) potentials in the *upward* current region of the auroral zone were initially inferred from satellite and rocket observations. Evidence includes detailed examination of precipitating electron distributions [6], observations of anti-Earthward ion beams [7] and observations of large-amplitude electric fields perpendicular to the magnetic field [8]. Recently, direct evidence of parallel electric fields has been reported [9]. In the *upward* current region of the aurora, the current is carried by electrons originating from a hot ($\sim$1 keV), tenuous (~ 1 cm^{-3}) plasma moving into a $\sim$500: 1 magnetic mirror created by the Earth's field. The source population is energized by approximately one to two orders of magnitude. Theoretical treatments on how collisionless plasmas support the inferred parallel potentials have been inconclusive. These treatments include large double layers [10], anomalous resistivity [11, 12], weak double layers [13] and magnetic mirror force [14, 15].

† Currently at Brown University, Providence, RI, USA.

0741-3335/99/SA0061+13$19.50

The recent discovery of quasi-static, parallel potentials in the *downward* current region of the auroral zone [1, 3] now show that naturally occurring, parallel potentials are responsible for particle acceleration in a clearly dissimilar plasma regime. The uncovering of two distinct plasmas that support parallel electric fields suggests that they may be a fundamental acceleration mechanism in astrophysical plasmas. In the *downward* current region, electron flow is from a cold (< 1 eV), higher density (10^3–10^6), collisionless plasma into a hot, tenuous plasma. Electrons are accelerated up to 10^4 times their initial thermal energy. There is no retarding magnetic mirror.

The FAST satellite also reported Debye (λ_D)-scale plasma structures associated with quasi-static, magnetic-field-aligned electric fields [4, 5]. The solitary structures were observed with energetic, field-aligned electron fluxes that were strongly modulated. The structures have electromagnetic signatures which are consistent with a positive spheroid ($\delta n/n \sim 10\%$) surrounded by a negative halo travelling at the electron drift velocity (v_{ed}). The electric field signal parallel to $\boldsymbol{B}_0$ is bipolar, almost always with the same sense, first in the direction of the electron drift velocity, then opposite. The measured scale-size parallel to the magnetic field is $\sim 2\lambda_D$. The perpendicular signal ($\Delta \boldsymbol{E}_\perp$) is unipolar and showed no preferred direction which indicates that the structures were 3D. The $\boldsymbol{E}_\perp$ spectra had depleted power at the H^+ cyclotron harmonics and solitary structures are occasionally organized near the H^+ cyclotron frequency. The magnetic perturbation ($\Delta \boldsymbol{B}$) is also unipolar, perpendicular and such that $|\Delta \boldsymbol{E}|/|\Delta \boldsymbol{B}| \sim c^2/v_{ed}$ and $\Delta \boldsymbol{E} \cdot \Delta \boldsymbol{B} = 0$, consistent with the Lorentz field of a moving charge.

Similar structures have been observed by other auroral spacecraft [16] and in space plasmas outside the aurora [17]. The solitary structures have speeds far greater than the ion thermal speed and thus were interpreted to be 'electron phase space holes' [18–20]. The FAST results demonstrated that the structures are 3D, Debye-scale charge clouds moving at the electron drift velocity, that they are inconsistent classical soliton solutions and that they facilitate ion–electron momentum exchange.

2. Parallel electric fields—upward current region

Observations of large-amplitude, perpendicular (to $\boldsymbol{B}_0$) electric fields in the auroral zone [8] have provided strong evidence of quasi-static, parallel potentials in the *upward* current region of the auroral zone. The correlation of anti-Earthward ion beams with these large-amplitude, perpendicular electric fields [21] and the qualitative agreement between the inferred parallel potential and ion beam energies [22, 23] suggested that parallel potentials are largely responsible for energizing auroral particles. Evidence of parallel electric fields also has been found in studies of electron distributions [6] and observations of ion beams [7].

2.1. Observations

The observations in this paper are from the FAST satellite which measures charged particle distributions and electromagnetic fields in the Earth's auroral zone from 300 km to 4175 km in altitude. The instruments are described elsewhere [24, 25]. The FAST satellite has orders of magnitude higher time resolution than previous missions, measuring electric and magnetic fields faster than $1/f_{pe}$ (and $1/f_{ce}$) and compiling particle distributions in $10/f_{pe}$ to $100/f_{pe}$, where f_{pe} and f_{ce} are the electron plasma and electron cyclotron frequencies.

We start with an overview of an auroral crossing. Figure 1 displays $\sim$50 s of high time resolution observations from a near-midnight, northern auroral crossing by the FAST satellite. During this time, the satellite moved $\sim$250 km northward across a visible auroral arc. The

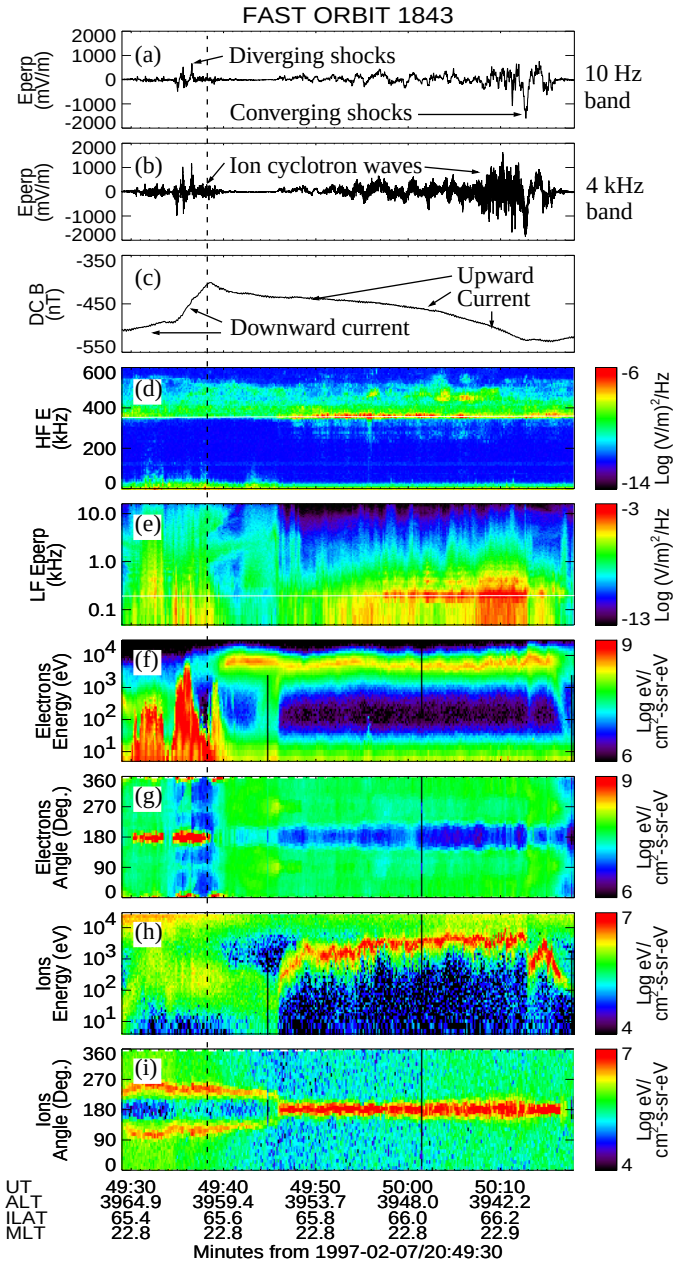

Figure 1. (From [1]) High-resolution observations of the near-midnight auroral zone. The broken line separates the downward and upward current regions. (a) The DC electric field signal filtered to 10 Hz, perpendicular to $\boldsymbol{B}_0$ and nearly along to the velocity of the satellite. (b) The DC electric field signal at ∼4 kHz bandwidth. There were strong ion cyclotron waves. (c) The nearly east-west component of the magnetic field. A positive slope indicates a downward current and a negative slope an upward current. (d)–(e) The high- and low-frequency power spectral density of the electric field against frequency. The white lines are the electron and H^+ cyclotron frequencies. (f), (g) Electron energy flux against energy and pitch angle. Fluxes near 180° are up-going and those near 0° or 360° are down-going. (h), (i) Ion energy flux against energy and pitch angle. Fluxes near 180° are up-going.

broken line separates the *downward* and *upward* current regions. For now, we concentrate on the *upward* current region on the right-hand side. The top panel (a) displays the perpendicular DC electric field at 10 Hz bandwidth that was nearly along the payload velocity vector (mostly northward). The most visible DC electric field in the *upward* current region had a positive signal from ∼20: 50: 08 UT to ∼20: 50: 12 UT followed by a large negative excursion at ∼20: 50: 12.7 UT.

Panel (b) of figure 1 shows the same DC electric field signal at ∼4 kHz bandwidth. Large-amplitude (∼1 V m^{-1} pp) waves obscure the DC electric field. Panel (c) displays the nearly east-west component of the DC magnetic field. The steep positive slope in the magnetic field indicates that there was an intense *downward* current in a narrow region. The negative slope reflects a less intense *upward* current which extended over a larger region. Panels (d) and (e) display the high- and low-frequency power spectral density of the electric field against frequency. The downward current region had strong, broadband emissions extending from ∼50 Hz to ∼20 kHz. There were intense ion cyclotron emissions in both regions.

Electron fluxes are displayed as a function of energy in panel (f) and pitch angle in panel (g). The *upward* current region (right-hand side) had precipitating electrons (20: 49: 40 UT to the end of the plot) with a mono-energetic peak at ∼10 keV that were mostly isotropic in pitch angle with a loss cone. From ∼20: 49: 46 UT on, there were no electron fluxes below ∼1 keV (fluxes $<$ 60 eV were spacecraft photo-electrons). The ion fluxes against energy and pitch angle are displayed in panels (h) and (i), respectively. An up-going, energetic ion beam dominates the upward current region. The precipitating electron fluxes and the ion beam indicate that particle acceleration was both above and below the spacecraft.

2.2. Test of the auroral model

Figure 2 displays an idealized model of the auroral acceleration region. The near-vertical broken curves represent the magnetic field and the thin full curves represent contours of constant potential. The basic idea is that there is a ∼10 kV potential drop along the magnetic field which accelerates the precipitating electrons and anti-Earthward ions. Under this model, the perpendicular electric fields surrounding the ion beam should be directed towards each other, called 'converging' electric fields.

A test of this model can be made with the high-resolution FAST data. In figure 2, a box is drawn with four segments labelled S1–S4. Segment S1 is at the edge of the ion beam, so we assume that there is no potential. Segment S2 is in the highly conducting ionosphere and should have only a small potential which we neglect. The potential along segment S3 can be determined from the ion beam energy. Under the static auroral model and Faraday's law, this must be opposite the potential along segment S4 which can be determined from the electric field observations.

Figure 3(a) shows an expanded view of the perpendicular DC electric field in the *upward* current region from figure 1. Panel (b) displays up-going ion fluxes with the inferred parallel potential superimposed. The parallel potential was derived by integrating the product of the observed electric field and the spacecraft velocity from the left edge of the ion beam (20: 49: 46 UT) where the parallel potential was assumed to be zero. We also assumed the parallel potential was zero at the right edge of the ion beam (20: 50: 13 UT) and imposed a constant ionospheric electric field. Except near 20: 49: 47 UT and 20: 49: 55 UT, the implied parallel potential and the ion beam energy are within ∼25% when the ion beam energy was greater than 500 eV. This detailed, quantitative agreement over a 30 s period implies that the ion beam was energized by a parallel potential that endured for tens of seconds. The FAST data provide strong support that quasi-static, parallel potentials are

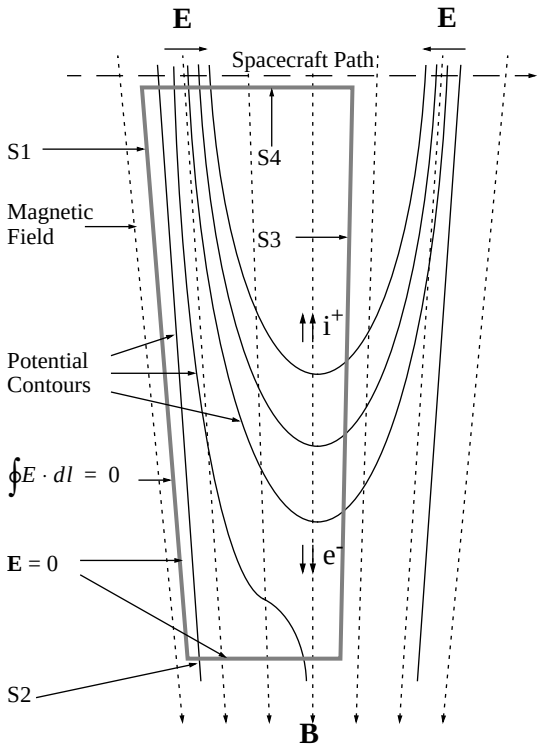

Figure 2. A model of the upward current region of the aurora. The nearly vertical short broken curves represent the Earth's magnetic field. The thin full curves are equipotential contours. The U-shaped potential contours form a ∼10 kV potential along the magnetic field. Electrons are accelerated Earthward and ions are accelerated anti-Earthward. Faraday's law can be applied to the thick-lined box. The potential along segments S1 and S2 is assumed to be zero. The potential along segment S3 can be estimated from the ion energy. The potential along S4 can be estimated by integrating the measured electric field along the spacecraft track. The potentials along S3 and S4 should be opposite each other under this model.

the primary mechanism for charge particle acceleration in the *upward* current region of the aurora.

3. Parallel electric fields—downward current region

One of the most important results of the FAST mission was to identify the 'reverse' aurora where electrons are accelerated anti-Earthward by quasi-static, parallel potentials in the *downward* current region [1, 3]. The *downward* current region model is similar to that of the upward current region, except that the electric fields are reversed and electrons are accelerated anti-Earthward. There is no corresponding visible auroral arc. Thus, this region has been labelled by some as the 'black aurora'.

Signatures of parallel potentials are clearly visible in the data. Perpendicular electric fields in the *downward* current region (figure 1(a), ∼20: 49: 37 UT) have a negative (nearly southward) electric field followed by a positive (nearly northward) electric field. This 'diverging' pattern is seen twice. The electrons (figures 1(f)–(g), left-hand side) were upgoing and were confined to very narrow pitch angles (180°) but had a broad energy range.

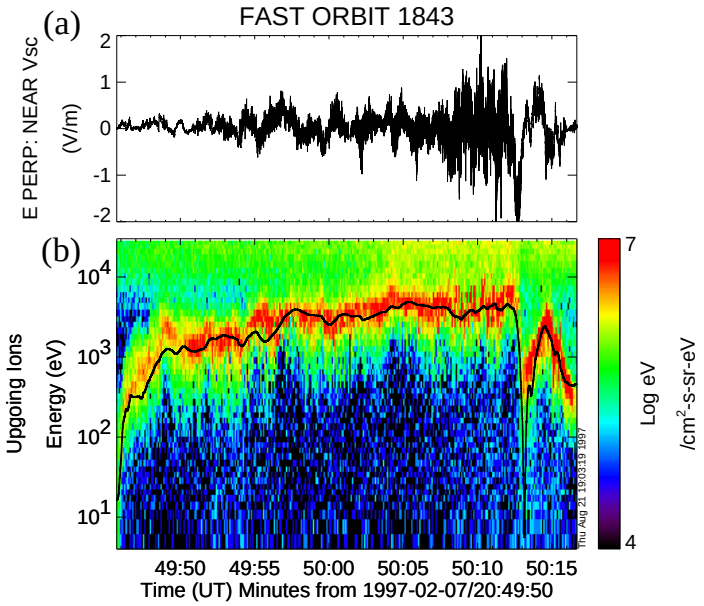

Figure 3. (From [1]) (a) The DC electric field perpendicular to $\boldsymbol{B}_0$ and nearly along to the velocity of the satellite. (b) Up-going ion energy flux against energy with the inferred parallel potential from the observed electric field superimposed.

Energetic ion fluxes (figures 1(h)–(i)) were concentrated at perpendicular pitch angles ($\sim$90° and $\sim$270°) distributions indicative of heating.

We can perform this same test to determine if parallel potentials are the primary energy source in *downward* current regions. The top panel of figure 4 displays the electric field. Below are the up-going electron fluxes with the inferred parallel potential superimposed. The broad energy peak in the up-going electron fluxes suggest that wave–particle interactions strongly modified the electron distribution. Nonetheless, the inferred parallel potential and the electron energy at the peak fluxes display similar characteristics and are often within a factor of two of each other.

The detailed agreement between inferred potentials from electric fields and particle energies in both current regions confirms that particle acceleration in the auroral zone is largely from parallel potentials. The parallel potentials appear to be stable on time scales of tens of seconds and over distances of tens of hundreds of kilometres. In the *upward* current region, the electrons flow from a hot plasma into a cold plasma and are accelerated to $\sim$10 to $\sim$100 times their thermal energy. In the *downward* current region, electrons flow from a cold, dense plasma into a hot plasma and are accelerated to up to 10^4 times their initial thermal energy. Thus, FAST observations now show that naturally occurring, quasi-static, parallel potentials accelerate electrons and ions in two distinct plasma regimes with distinct supporting mechanisms.

4. Solitary structures

One of the important questions in auroral physics is how quasi-static, parallel potentials are maintained in a collisionless plasma. In the upward current region, the magnetic mirror force

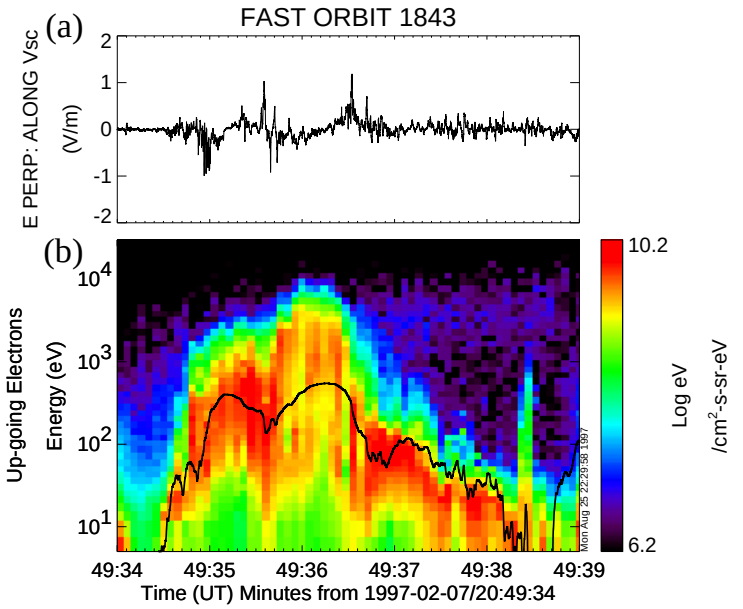

Figure 4. (From [1]) (a) The DC electric field perpendicular to $\boldsymbol{B}_0$ and nearly along to the velocity of the satellite. (b) Up-going electron energy flux against energy with the inferred parallel potential from the observed electric field superimposed.

and a dearth of charge carriers could account for some, but not all, of the resistance. The downward current region is quite different. Electrons are accelerated by as much as 10^4 times their thermal energy, there is no resistive mirror force and the cold, dense, ionospheric plasma provides an ample supply of charge carriers. Resistivity must come from the collective behaviour of the plasma.

The electron distributions in the *downward* current region appear to be strongly modified by wave–particle interactions (figure 1(f)). Wave observations from the FAST satellite in the *downward* current region reveal large-amplitude electromagnetic structures. These structures travel at speeds far greater than the ion acoustic speed and have amplitudes as high as 2.5 V m^{-1} (nonlinearities are expected) which distinguishes them from previous observations of ion-acoustic solitary waves or weak double layers [13]. They are typically observed in or near regions where parallel electric fields accelerate electrons and are associated with strong modulations in both up-going and down-going electron fluxes.

4.1. Observations

In the regions that had up-going, energetic, field-aligned electron fluxes (figures 1(f), (g), 20: 49: 30 UT–20: 49: 40 UT), there were bursts of broadband VLF (kHz) emissions (figures 1(d),(e))). The enhanced VLF emissions appeared in both the perpendicular and parallel electric field. The parallel electric field (figure 1(d)) had enhanced broadband noise above 1 kHz. The perpendicular electric field (figure 1(e)) had similar enhanced broadband noise but also had lower frequency (∼200 HZ–∼1 kHz) emissions that exhibited depletions in power or 'bite-outs' at the H^+ cyclotron harmonics (see, [1], figure 4). There was also a weak perpendicular magnetic component (not displayed). These broadband emissions are the result

of a series of solitary structures.

Figure 5 displays the electromagnetic fields of the solitary structures (from a different orbit than figure 1). Panels (a)–(d) display the parallel electric field ($\Delta E_\parallel$), two components ($\Delta E_\perp$) perpendicular to the ambient magnetic field ($\boldsymbol{B}_0$) and one component of the perturbation of the magnetic field ($\Delta B_\perp$) perpendicular to $\boldsymbol{B}_0$. Panels (aa)–(dd) are expanded views of panels (a)–(d). $\Delta E_\parallel$ was bi-polar, almost always with the same sense. The first excursion (negative) was in the direction of the energetic electron drift. The second excursion (positive) was opposite the direction of the electron drift. The duration of the solitary structures was $\sim$100 μs. Both components of $\Delta E_\perp$ were unipolar with comparable amplitudes. $\Delta B_\perp$ was also unipolar and such that $\Delta E_\perp / \Delta B_\perp \gg c$.

The velocity of the structures ($v_{\rm delay}$) was measured by time delays between physically separated antennae. An example of the time delay data is displayed in figure 6. The measured speeds almost always lie between 500 km s^{-1} and 5000 km s^{-1}. The structures travel in the same direction as the energetic electrons at a velocity that corresponds to the electron drift velocity derived from the observed electron distributions

$$v_{\rm ed} = \int f_{\rm e}(\boldsymbol{v}) \boldsymbol{v}\, {\rm d}v^3 / n \tag{1}$$

where $f_{\rm e}$ is the electron distribution function and n is the plasma density. Over a large (> 1000) sample of events, the measured velocity $v_{\rm delay}$ was found to be within a factor of two of $v_{\rm ed}$ approximately 50% of the time. In contrast, the ratio $v_{\rm delay}/v_{\rm eth}$, where $v_{\rm eth}$ is the electron thermal velocity, was typically $\sim$1/3. It was also found that $\Delta B_\perp$ is constant with the Lorentz field of a moving charge such that $v_{\Delta B} \cong v_{\rm delay}$, where $v_{\Delta B} = c^2 \Delta B_\perp / \Delta E_\perp$ (the electrons were non-relativistic). The data were consistent with $\Delta \boldsymbol{E} \cdot \Delta \boldsymbol{B} = 0$. The evidence demonstrates that the solitary structures were electrostatic and moving at less than $v_{\rm eth}$ in the electron drift frame. The structure velocities are substantially greater than the ion thermal speed.

The electromagnetic signature is that of a two- or three-dimensional positive charge (or electron hole) passing by the spacecraft at the electron drift velocity. Although auroral arcs typically display two-dimensional structure at large scales, $\Delta E_\perp$ showed no preferred direction, suggesting that the structures were 3D. In addition, $\Delta E_\parallel$ and $\Delta E_\perp$ were typically comparable and hodegrams of $\Delta E_\parallel$ against $\Delta E_\perp$ often conform to a spheroid such that $z_0 \leqslant r_0$, where z_0 is the parallel (to $\boldsymbol{B}_0$) scale size and r_0 the perpendicular scale size. It was suggested [5] that the oblateness of the spheroids depends upon the ratio of ion gyroradius ($\rho_{\rm i}$) and Debye length ($\lambda_{\rm D}$) which typically falls between two and 20 ($2 < \rho_{\rm i}/\lambda_{\rm D} \leqslant 20$) in regions where the structures were observed.

4.2. Parallel size

The parallel scale size of the solitary structures can be determined from their motion. A speed of $\sim$2000 km s^{-1} and a duration of 100 μs implies the typical structure size is $\sim$200 m parallel to $\boldsymbol{B}$, only a few Debye lengths ($\lambda_{\rm D}$ is $\sim$10 m to $\sim$100 m). Figure 7(a) is a greatly expanded view of $\Delta E_\parallel$. The time axis has been translated into Debye lengths assuming a constant parallel velocity. The displayed structure had a small $\Delta E_\perp$ which indicates that it was almost centred about the spacecraft as it passed by. The local plasma had the following conditions: $n_0 = 5.7 \pm 2.0$ cm^{-3}, $T_{\rm e\parallel} = 704 \pm 145$ eV, $v_{\rm sol} = 3.2 \times 10^6 \pm 1.1 \times 10^6$ m s^{-1}, $T_{\rm i\perp} = 370 \pm 74$ eV, $|\boldsymbol{B}_0| = 11481 \pm 10$ nT, $\lambda_{\rm D} = 82 \pm 30$ m, $\rho_{\rm H^+} = 241 \pm 24$ m. The measured signal fit remarkably well to a derivative of a Gaussian

$$E(z) = \frac{E_0 z}{z_0} {\rm e}^{1/2 (z/z_0)^2}. \tag{2}$$

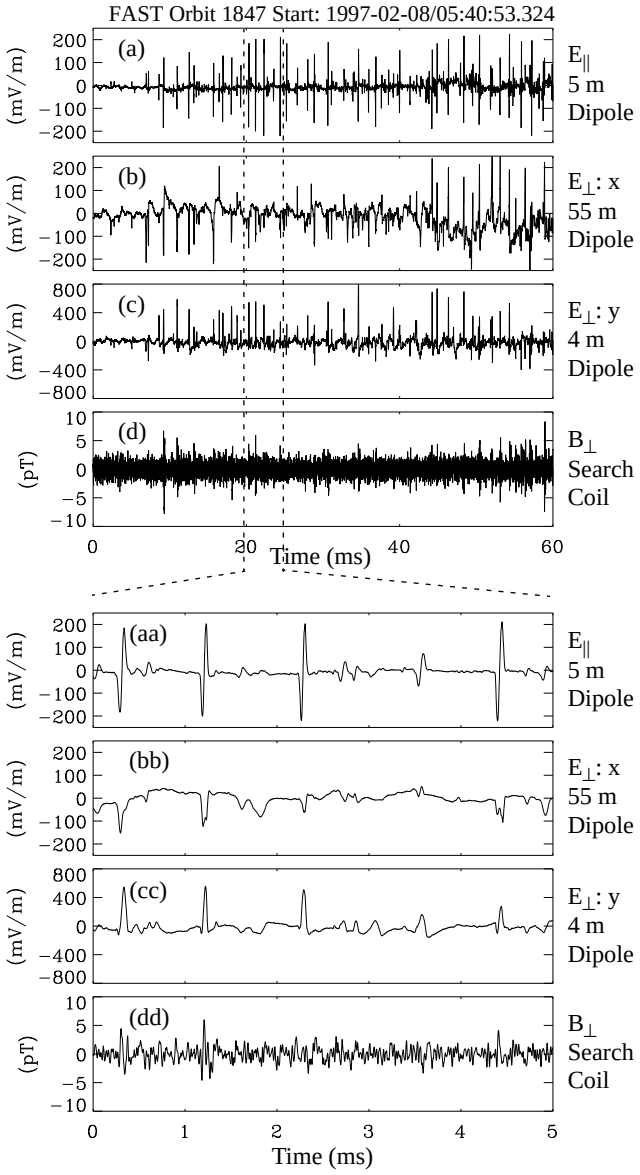

Figure 5. (From [5]) (a) The electric field parallel to $\boldsymbol{B}_0$. (b) The electric field perpendicular to $\boldsymbol{B}_0$ ($\Delta E_\perp$) and in the spin plane of the satellite. This signal, measured by a 56 m dipole antenna, appears attenuated, indicating that the structure size may have been < 112 m. (c) $\Delta E_\perp$ along the spin axis of the satellite. (d) A perturbation magnetic field perpendicular to $\boldsymbol{B}_0(\Delta B_\perp)$. $\Delta B_\perp$ was filtered to a pass band (3 kHz–16 kHz) to expose the weak signals and therefore may not appear unipolar in this figure. (aa)–(dd) An expanded view of this data.

The full curve in figure 7(a) is a fit to the data (circles) with $z_0 = 0.7 \pm 0.3\lambda_D$.

The charge density of the structures can be derived from the fit (figure 7(b)). The actual charge density lay between the two traces which represent the extremes, spherical and planar geometry. The structures have a positive core of roughly 5% n_0 surrounded by a negative halo. A close examination of $\Delta E_\parallel$ (figure 3(a)) reveals that it abruptly begins and ends which

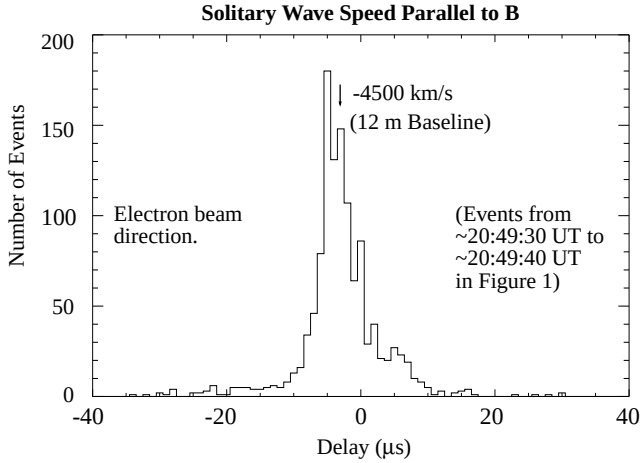

Figure 6. (From [4]) A histogram of the measured parallel delay between solitary wave signals from dipoles separated by 12 m. There were 1196 solitary wave events greater that 50 mV m^{-1} in a 10 s period during orbit 1843. The average and median delay indicates a typical speed of $\sim$4500 km s^{-1} anti-Earthward. The delay was calculated by correlating signal pairs (sampled at $\sim$30 μs) over two spin periods to eliminate systematic errors. Random errors were typically $\sim$2 μs. A similar analysis with a smaller number of samples from 0.5 μs resolution data has verified the structures move with the electron beam typically between 500 km s^{-1} and 5000 km s^{-1}.

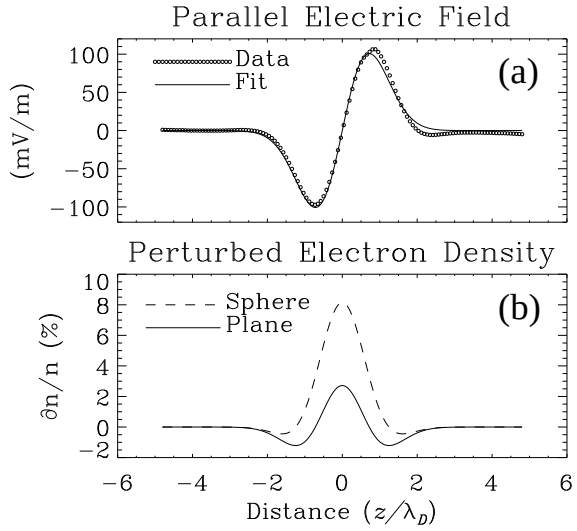

Figure 7. (From [5]) (a) $\Delta E_{\parallel}$. The dotted curve represents the data at 0.5 μs resolution translated into Debye lengths assuming a constant parallel velocity, $v_{\rm sol} = 3.2 \times 10^6 \pm 1.1 \times 10^6$ m s^{-1}. The full curve is the fit to equation (2). (b) Calculated charge densities assuming spherical and planar geometry.

implies that the structures are, in total, neutral.

We examined over 1000 events to determine the average size (Gaussian half-width, z_0) of the structures parallel to $\boldsymbol{B}_0$. The solitary structures were chosen by an algorithm that was optimized to ensure the selected events were solitary structures. The algorithm, however, did

not find all of the events. The primary selection criteria isolated bipolar, parallel electric field signals with peaks exceeding the surrounding root mean square (RMS) amplitude, averaged over ∼2 ms, by a factor of five. The perpendicular electric field had to be nearly unipolar. A spot check indicated ∼97% of the structures identified by the search algorithm were as described, but over one half of the structures discernible by eye were not identified, especially those with low amplitudes.

The results are plotted in figure 8. λ_D was determined from the measured electron temperature and the ion density (the ion density measurement had the best accuracy). The scale size was estimated as $\Delta t_{pp} v_{sol}/2$ where Δt_{pp} is the time between the positive peak and negative peak and v_{sol} is the velocity of the solitary structure. In most cases, λ_D and Δt_{pp} were determined to better than 25%. v_{sol} could not be as accurately determined. The measured value (v_{delay}) was used if the antennae were favourable. The Lorentz velocity ($v_{\Delta B}$) was used if $\Delta B_\perp$ was detectable. The average scale size was $1.80\lambda_D$ with a standard deviation of $1.13\lambda_D$. The standard deviation was influenced by the uncertainty in v_{sol}.

4.3. Properties

The relationship between the amplitude and the size of the solitary structures may give some insight into their origin. Under a simple self-focusing process, for example the Korteveg–Devries solution or Zacharov solution, the amplitude should increase with decreasing size of the solitary structure. Other solutions, such as a one-dimensional (1D) 'electron phase space hole' solution [20] predict the opposite.

The relationship between maximum potential of the observed solitary structures (Φ_0) and size (z_0) is displayed in figure 9. Φ_0 clearly increases with size. The general shape of the curve, when $z_0/\lambda_D < 2$, agrees with analytical results and particle simulations of a 1D 'electron phase space hole' [20]. The observed structures are predicted to be stable in one dimension if their velocity is less than twice the electron thermal speed [20]. The observed structures satisfy that criteria.

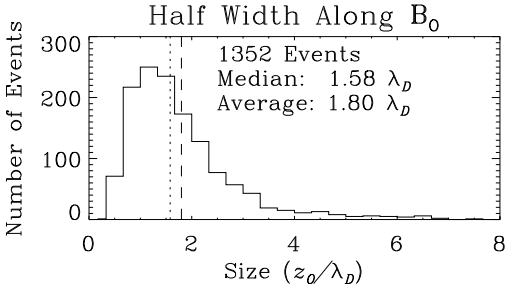

Figure 8. (From [5]) A histogram of the occurrence of solitary structures against their size. The standard deviation in size is influenced by uncertainties in the velocity measurement.

The structure properties parallel to $\boldsymbol{B}_0$ can be understood as a pure electron phenomena in one dimension. The 1D assumption has validity because the electrons are strongly magnetized ($\rho_e \ll \lambda_D$). In these examples, $\rho_e < 1$ m and $\lambda_D \sim 100$ m. The observations, however, clearly indicate the structures are multi-dimensional. Theoretically, one expects ions to control the perpendicular scale size.

The perpendicular scale size has been difficult to establish. While not definitive, the observational evidence also suggests that ion dynamics play a role. The structures were occasionally periodically spaced close to the H^+ cyclotron frequency, which was also very near

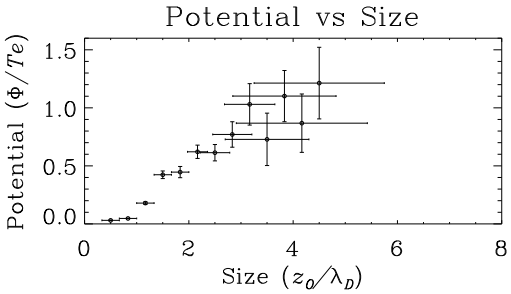

Figure 9. (From [5]) The peak potential against the structure size. Each point reflects the mean potential and size averaged over a size bin in figure 8.

the lower hybrid frequency [5]. The spectral power density of the electric field waveforms, however, almost always shows structure at the H^+ cyclotron harmonics [1]. Finally, the solitary structures were observed in sets. The spatial extent of the sets perpendicular to the magnetic field (under the assumption that they occupied the same magnetic flux tube and were not a temporal phenomena) was often several H^+ Larmor radii. The observations suggest that the perpendicular dimension scales with ρ_i.

4.4. Ion heating

Resistance in a collisionless plasma comes from momentum exchange between electrons and ions. The 3D character of the solitary structures naturally provides such resistance. In the frame of the solitary structure, ions are incident at very high velocity compared to their thermal velocity and will scatter from the positively charged core. The scattering angle is small and should be treatable by the Vlasov equation. We instead provide a simple estimate. Assuming the perturbation to the ion trajectory is small and that the ion are unmagnetized (in other words, the ion transit time is far less than the gyroperiod), the perpendicular impulse from a proton passing through the solitary structure with an impact parameter of r is

$$M\Delta v_{i\perp}(r) = \int_{-\infty}^{\infty} eE_{\perp}(r, z(t))\mathrm{d}t \tag{3}$$

where M is the proton mass. Assuming the solitary structure does not recoil, the parallel velocity of the ion will undergo a second-order perturbation $\Delta v_{i\parallel} \cong -\delta v_{i\perp}^2/2v_{sol}$, resulting in a parallel momentum exchange with the electrons.

This analysis can be applied directly to the observations. There are two noteworthy results from this exercise. In the frame of the ions, the perpendicular energy gain is a significant fraction of the ion thermal energy. At the rate that the structures are observed, ions should receive substantial perpendicular heating, consistent with the observations (figures 1(h),(i)). The change in ion momentum must be absorbed by electrons which requires a parallel electric field if the structures are in steady state.

5. Conclusions

In summary, FAST observations verified that parallel potentials are the primary acceleration mechanism in the *upward* current region and now show that naturally occurring, quasi-static, parallel potentials accelerate electrons and ions in two distinct plasma regimes with distinct supporting mechanisms. The detailed agreement between inferred potentials of the electric

fields and particle energies in both current regions confirms that particle acceleration in the auroral zone is primarily from quasi-static, parallel potentials. These observations suggest that quasi-static, parallel electric fields may be a fundamental particle acceleration mechanism in astrophysical plasmas.

Debye-scale solitary structures associated with quasi-static, magnetic-field-aligned electric fields were demonstrated to be 3D 'electron holes' travelling at the electron drift velocity. The parallel profile fits very well to a Gaussian, the parallel size increasing with increasing potential. The structures are unique in that they exist in a strongly magnetized plasma and are multi-dimensional. Evidence suggests that ion motion influences the perpendicular scale size and organizes sets of the structures. The 3D nature of the structures can lead to a strong interaction with ions through small-angle scattering from the positive core. Through scattering, the ions can receive considerable transverse heating and an appreciable exchange of momentum with the electrons. These findings provide evidence that Debye-scale solitary structures may play a role in supporting large-scale parallel potentials.

References

[1] Ergun R E *et al* 1998 *Geophys. Res. Lett.* **25** 2025
[2] McFadden J P *et al* 1998 *Geophys. Res. Lett.* **25** 2021
[3] Carlson C W *et al* 1998 *Geophys. Res. Lett.* **25** 2017
[4] Ergun R E *et al* 1998 *Geophys. Res. Lett.* **25** 2041
[5] Ergun R E, Carlson C W, McFadden J P, Mozer F S, Muschietti L and Roth I 1998 *Phys. Rev. Lett.* **81** 826
[6] Evans D S 1974 *J. Geophys. Res.* **79** 2853
[7] Shelley E G, Sharp R D and Johnson R G 1976 *Geophys. Res. Lett.* **3** 654
[8] Mozer F S, Carlson C W, Hudson M K, Torbert R B, Parady B, Yatteau J and Kelley M C 1977 *Phys. Rev. Lett.* **38** 292
[9] Mozer F S and Kletzing C A 1998 *Geophys. Res. Lett.* **25** 1629
[10] Block L P 1972 *Cosmic Electrodyn.* **3** 349
[11] Hudson M K and Mozer F S 1978 *Geophys. Res. Lett.* **5** 131
[12] Ishiguro S, Sato T, Takamaru H and The Complexity Simulation Group 1997 *Phys. Rev. Lett.* **78** 4761
[13] Temerin M, Cerny K, Lotko W and Mozer F S 1982 *Phys. Rev. Lett.* **48** 1175
[14] Knight S 1973 *Planet. Space Sci.* **21** 741
[15] Chiu Y T and Schultz M 1978 *J. Geophys. Res.* **83** 629
[16] Mozer F S, Ergun R E, Temerin M, Cattell C A, Dombeck J and Wygant J 1997 *Phys. Rev. Lett.* **79** 1281
[17] Matsumoto H, Kojima H, Miyatake T, Omura Y, Okada M, Nagano I and Tsutsui M 1994 *Geophys. Res. Lett.* **21** 2915
[18] Omura Y, Kojima H and Matsumoto H 1994 *Geophys. Res. Lett.* **21** 2923
[19] Schamel H 1982 *Phys. Scr.* **T2/1** 228
[20] Turikov V A 1984 *Phys. Scr.* **30** 73
[21] Bennett E L, Temerin M, Mozer F S and Boehm M H 1983 *J. Geophys. Res.* **88** 7107
[22] Redsun M S, Temerin M, Mozer F S and Boehm M H 1985 *J. Geophys. Res.* **90** 9615
[23] Temerin M, Boehm M H and Mozer F 1981 *Geophys. Res. Lett.* **8** 799
[24] Carlson C W, Pfaff R and Watzin J G 1998 *Geophys. Res. Lett.* **25** 2013
[25] Carlson C W and McFadden J P 1998 *Monog. Meas. Techn. Space Plasma* ed R Pfaff AGU